PNAS
www.pnas.org

Supplementary Information for

Rhodopsin-mediated Light-off-induced Protein Kinase A Activation in Mouse Rod Photoreceptor Cells.

Shinya Sato[a*], Takahiro Yamashita[b], and Michiyuki Matsuda[a,c]

[a]Laboratory of Bioimaging and Cell Signaling, Graduate School of Biostudies, Kyoto University, Kyoto 606-8501 Japan;

[b]Department of Biophysics, Graduate School of Science, Kyoto University, Kyoto 606-8502 Japan;

[c]Department of Pathology and Biology of Diseases, Graduate School of Medicine, Kyoto University, Kyoto 606-8501 Japan;

*To whom correspondence should be addressed: Shinya Sato

Address: Laboratory of Bioimaging and Cell Signaling, Graduate School of Biostudies, Kyoto University, Kyoto 606-8501 Japan;

TEL: +81-75-753-9450

Email: sato.shinya.7e@kyoto-u.ac.jp

This PDF file includes:

Supplementary Text
Supplementary Methods
Figures S1 to S4
Legends for Movies S1 to S9
SI References

Other supplementary materials for this manuscript include the following:

Movies S1 to S9

www.pnas.org/cgi/doi/10.1073/pnas.2009164117

Supplementary Text

Estimated amount of photopigment activation by two-photon imaging.

There are three pathways for the rhodopsin activation and bleaching during two-photon imaging; direct single-photon and two-photon activations by the excitation light (direct 1P excitation, direct 2P excitation), and an indirect excitation by the emission from the fluorescent probe(s) (1). We have estimated the direct and indirect photopigment activation rates in a single imaging scan as 4×10^2 R* rod^{-1} and 1×10^3 R* rod^{-1}, respectively. These values are clearly smaller than the values that are required for the light-off-induced PKA activation.

We will describe how these rates were obtained. First, we estimated the direct 1P and 2P activations in our typical imaging set up using the light-adapted retinal explant. Based on the spectral sensitivity of the mouse rod in the infrared region (2), we assumed that the 1P excitation is dominant at 800 nm, whereas the 2P excitation becomes dominant at 900 nm. Unfortunately, sensitivity at 840 nm, which was used in our study, was not reported. Although the ratio of contribution is not clear, here, we assumed that 1P and 2P excitations have comparable contributions at 840 nm.

The Govardovskii template (3) was used to estimate the 1P activation efficiency. When the rhodopsin template (λ_{max} 500 nm) is extended to 840 nm, the relative absorbance efficiency is 2.4×10^{-9} to the maximum (Fig. S5*A*). The excitation laser power in our typical imaging was 8 mW at the sample plane. The power of the photon at 840 nm is 2.4×10^{-19} (J), which is obtained from the equation $E = hc/\lambda$, where E is the energy of a photon, h is the plank constant ($6.62607015 \times 10^{-34}$), c is the speed of light in vacuum (3.0×10^{-8} m s^{-1}), and λ is the wavelength (8.4×10^{-7} m). Thus, the average photon flux of the excitation laser is $(8.0 \times 10^{-3}) / (2.4 \times 10^{-19}) \approx 3.3 \times 10^{16}$ photons s^{-1}, and the photon density at the sample, based on the pixel dwelling time (8 µs) and the pixel size (0.17 µm^2), is $(3.3 \times 10^{16}) \times (8 \times 10^{-6}) / (0.17) \approx 1.6 \times 10^{12}$ photons µm^{-2}. Using the relative absorbance efficiency above, the 1P excitation in one scan of 840 nm laser is

comparable to $(1.6 \times 10^{12}) \times (2.4 \times 10^{-9}) \approx 3.8 \times 10^{3}$ photons μm^{-2} flash of 500 nm light. By multiplying the collecting area of a mouse rod, 0.47 μm^2 (4), rhodopsin activation was estimated as 1.8×10^{3} R* rod^{-1}, when the retina is dark-adapted and contains ~100% rhodopsin. However, in our light-adapted retinal explant, unbleached photopigments were approximately 8% rhodopsin and 8% isorhodopsin (Fig. 5*D*). Quantum yield of isorhodopsin is about 1/3 to that of rhodopsin (5). Therefore, estimated 1P excitation in our light-adapted retinal explant is $(1.8 \times 10^{3}) \times (0.08 + 0.08/3) \approx 1.9 \times 10^{2}$ R* rod^{-1}. Assuming that 1P and 2P excitations have comparable contributions, we estimated the total direct excitation rate as approximately 4×10^{2} R* rod^{-1}.

Next, we estimated the indirect activation. Because imaging was mainly done from PRS, we assumed that the AKAR3EV fluorescence is absorbed by rhodopsin without any attenuation. To obtain the relationship between photon emission and the pixel intensity of fluorescent image, calibrated 475 nm or 535 nm light from the light stimulation device (Fig. S4) was injected directly into the objective lens (Fig. S5*B*), and the light was detected with the CFP Ch detector (460-500 nm) or FRET Ch detector (520-560 nm), respectively, with an 8 µs of the pixel dwelling time (Fig. S5*C*). Then, mean intensities of images were plotted as a function of the photon number per pixel (Fig. S5*D*). Using this relationship, a mean CFP Ch pixel intensity in our typical imaging, 300, was converted to 6×10^{2} photons $pixel^{-1}$. The FRET Ch sensitivity was 94% of the CFP Ch sensitivity; this value will be used later for a calibration.

In the real specimen, fluorescent emission is supposed to be radiated toward random directions so that only a part of them are collected by the objective lens. Based on the numerical aperture of the objective lens (1.05) and the refractive index of the DMEM/F12 medium (1.34), the objective aperture angle is calculated as 0.90 radians, and the fraction of the photon collection was estimated as $(0.90 \times 2) / (2\pi) \approx 0.29$. Thus, the estimated total photon emission from the AKAR3EV is $(6 \times 10^{2}) / 0.29 \approx 2 \times 10^{3}$ photons $pixel^{-1}$.

Because the photon number so far is estimated only for those detected by the CFP Ch detector (i.e. photons in 460-500 nm range), we expanded this for the whole emission spectrum of the AKAR3EV. The emission spectrum of the AKAR3EV was predicted by summing up those of mTurquoise and YPet (Fig. S5*E*) which comprise the AKAR3EV. The YPet spectrum was then scaled based on the basal FRET/CFP of PRS layer (1.24; Fig. 2*B*, PRS of the light-adapted retina). Considering the detector sensitivity ratio above, the ratio of the area corresponding to FRET Ch and CFP Ch was adjusted at 1.24 / 0.94 = 1.32. The whole spectrum was further scaled up to set the area for the CFP Ch to the above estimated photon number, 2×10^3 (Fig. S5*F*). Finally, the effect of the AKAR3EV fluorescence on the rhodopsin activation was estimated by multiplying the normalized absorbance spectrum of rhodopsin (Fig. S5*G*), which converts the photon number of each wavelength into the corresponding number at 500 nm. The area of this calibrated spectrum is comparable to 5×10^3 photons pixel^{-1} of 500 nm light (Fig. S5*H*). Using the pixel size (0.17 μm^2), this value was converted to $(5 \times 10^3) / (0.17) \approx 3 \times 10^4$ photons μm^{-2}. Using the collecting area (0.47 μm^2) and the fractions of rhodopsin and isorhodopsin in our light-adapted retinal explant (8% each), the value was further converted as described earlier, to obtain the total indirect excitation rate of 1×10^3 R* rod^{-1}.

The photon density estimated for direct and indirect activations are in the order of 10^3 and 10^4 photons μm^{-2}, respectively, at 500 nm. On the other hand, the half saturating light intensity of the light-off-induced PKA activation was 6.5×10^7 photons μm^{-2} at 500 nm (Fig. S3*B*). Therefore, the impact of imaging technique is thought to be negligible, at least on the PKA activation.

Supplementary Methods

Ethical approval. The animal protocols were reviewed and approved by the Animal Care and Use Committee of Kyoto University Graduate School of Medicine (MedKyo17539, 17539-2, 18086, 19090, and 20081) and methods were carried out in accordance with the relevant guidelines and regulations.

Reagents. Dulbecco's modified Eagle's medium/nutrient mixture F-12 Ham (DMEM/F12; D2906, Sigma-Aldrich, St. Louis, MO, USA) supplemented with 1% (v/v) Penicillin-Streptomycin (26253-84; Nacalai Tesque, Kyoto, Japan) was prepared just before the imaging experiment. The medium was warmed up in a 40 °C water bath and bubbled with an O_2 and CO_2 gas mixture. The pH was monitored with a pH tester (HI98100; HANNA Instruments, Woonsocket, RI, USA), and the CO_2 concentration was adjusted to obtain pH 7.2-7.4. For the cone-specific staining in Fig. 1*I*, PNA-rhodamine (RL-1072; Vector Laboratories, Burlingame, CA, USA) was added to DMEM/F12 medium at 0.2% (v/v). Forskolin (F-500; Alomone Labs, Jerusalem, Israel) was dissolved in dimethyl sulfoxide (DMSO) at 50 mM and kept at -20 °C until used. Dopamine (040-15433; FUJIFILM Wako Pure Chemical, Osaka, Japan) was dissolved in ultrapure water at 1 mM and kept at -80 °C until used. 4-(2-hydroxyethyl)-1-piperazineethanesulfonic acid (HEPES) and NaCl were purchased from Nacalai Tesque. NaOH and hydroxylamine hydrochloride were from FUJIFILM Wako Pure Chemical. *n*-Dodecyl-β-D-maltoside (DDM) was from Dojindo (Kumamoto, Japan). Reagents for retinoid extraction and HPLC analysis (dichloromethane, *n*-hexane, Na_2SO_3, diethyl ether, isopropanol and benzene) were from FUJIFILM Wako and Nacalai Tesque. The genomic DNA extraction kit (69504; DNeasy Blood and Tissue Kit) was from Qiagen (Hilden, Germany). PCR reagents were from TaKaRa Bio (Kusatsu, Japan) and Toyobo (Osaka, Japan). PCR primers were from Fasmac (Atsugi, Japan).

Animals. Mice (*Mus musculus*) were housed in a specific-pathogen-free facility with a 14/10 hour light-dark cycle, fed a standard laboratory chow diet and water *ad libitum*, and used at the age of 1–6 months. Both male and female mice were used. Two or more animals were used for every experiment to confirm the reproducibility. PKAchu (C57BL/6J (B6J) background, nbio185; NIBIOHN, Osaka, Japan) and PKAchu-NC (C57BL/6J (B6J) background, nbio186) transgenic mice were backcrossed with B6 albino mice (Charles River Laboratories Japan, Yokohama, Japan) for more than 9 generations and used as albino PKAchu and albino PKAchu-NC, respectively. Transgene-positive, heterozygous mice were selected by visual inspection of their body fluorescence and used for both breeding and imaging. Wild-type PKAchu and PKAchu-NC were generated by crossing those albino mice with normal pigmented B6J mice (Charles River Laboratories Japan) for 3-7 generations, except for PKAchu used in the experiment shown in Fig. 1, which was crossed for only 1 generation. Removal of both the *rd8* mutation (a single base deletion at nt3481 on *Crb1*) (6) and the albino mutation (a G291T point mutation on *Tyr*) (7) was verified by Sanger sequencing of genomic DNA extracted using the DNeasy Blood and Tissue Kit (Qiagen). The following primers were used: for *rd8* genotyping, 5'-ACCTGATGGGTTCCCAATTG-3' (forward) and 5'-AACCAGCCTTGTTTAGCACC-3' (reverse); for albino genotyping, 5'-GGGGTTGCTGGAAAAGAAGTCTGTG-3' (forward) and 5'-TGTGGGGATGACATAGACTGAGCTG-3' (reverse). PKAchu *Gnat1*$^{+/-}$ and PKAchu *Gnat1*$^{-/-}$ were obtained by crossing wild-type PKAchu with *Gnat1*$^{-/-}$ mice (B6J background; the kind gift of Dr. Vladimir J. Kefalov) (8) for 2-3 generations. For genotyping *Gnat1*, genomic DNA was extracted by incubating a biopsy sample in 50 µL of 0.1 M NaOH (1 hour, 95 °C). The sample was then neutralized by adding 50 µL of 1 M Tris-HCl (pH 7.5) and centrifuged (15300 ×g, 1 min, 25 °C). The resulting supernatant was used as a template for a genotyping PCR. The following primers were used: for the *Gnat1* wild-type allele, 5'-GGCTTTCTTCAGGGGTCTTA-3' (forward) and 5'-

GGCAGGGTAGTGGTTGTGAA-3' (reverse); for the *Gnat1* knockout allele, 5'-CATTCGACCACCAAGCGAAACATC-3' (forward) and 5'-ATATCACGGGTAGCCAACGCTATG-3' (reverse). Taken together, the genetic background of PKAchu and PKAchu-NC used in this study is normal pigmented B6J except for albino PKAchu and PKAchu-NC that have the B6 albino background.

Preparation of the retinal explants for imaging. The following tools were used in the retina dissection: a stereomicroscope (SZX16; Olympus, Tokyo), curved forceps (91197-00; Fine Science Tools, Foster City, Canada), micro-scissors (15009-08; Fine Science Tools) and two fine forceps (11251-20; Fine Science Tools). For dark-adapted retinas, a mouse was kept in darkness overnight and the preparation was done under dim red light. For light-adapted retinas, a mouse was kept under normal room illumination (white light, 200-300 lux) for more than 1 hour and the explants were prepared under the same lighting condition. The relative amount of unbleached photopigments in this explant was constantly about 16% to that of rhodopsin in the dark-adapted control for wild-type (Fig. 5A) and was below the detection limit for albino (Fig. 6A). If not otherwise specified, imaging data were obtained from light-adapted retinal explants. A mouse was killed under isoflurane anesthesia. Eyes were enucleated with curved forceps and hemisected to remove the cornea, vitreous and lens. Eyecups thus obtained were transferred into a 35-mm culture dish filled with 2 mL DMEM/F12 medium and cut radially from three or four points. The retina was peeled off with fine forceps and transferred onto a culture insert (PICMORG50; Merck Millipore, Billerica, MA, USA) which was pre-wet with DMEM/F12. The retina was flat-mounted ganglion cell-side up and tightly adhered onto the culture insert with suction (9) to prevent positional drift and detachment during time-lapse imaging. The culture insert was then fixed in a custom perfusion chamber made of acrylic glass (width 40 mm, depth 33 mm, height 10 mm) or a square polystyrene dish (1-4698-01; As One, Osaka, Japan). The entire preparation process was completed in less

than 20 min after administration of anesthesia. For the cone-labeling in Fig. 1*I*, the culture insert with a retinal explant was placed onto 1 mL DMEM/F12 supplemented with 0.2% (v/v) PNA-rhodamine, pre-incubated in a humidified CO_2 incubator at 37 °C for 1 hour, and then washed once with DMEM/F12 just before the imaging (10).

Perfusion equipment. The perfusion chamber was placed on an electromotive microscope stage (MPT-AS01-FV; SIGMA KOKI, Hidaka, Japan) with a heating pad (MP-908-N; Makami Denshi, Kishiwada, Japan). The retina in the chamber was perfused with oxygenated DMEM/F12 medium delivered at 1 mL/min using a double-head peristaltic pump (AC-2110 II; ATTO, Tokyo) and warmed up with an inline heater (an SF28 heater controlled by a TC344B temperature controller; Warner instruments, Hamden, CT, USA) (Fig. 1*A*). Medium was continuously drained from the chamber with the same pump. The drain rate was adjusted to be slightly higher than 1 mL/min to prevent overflow. The heater voltage was adjusted manually to maintain the temperature in the dish at 33-35 °C (11), which was monitored by a K-type thermocouple probe (AD-1214; A&D, Tokyo) attached near the tip of the objective lens. Temperature data was imported to a computer via a breakout board (MAX31855; Adafruit, New York, NY) and an Arduino UNO microcontroller board (Arduino, Turin, Italy). Temperature was recorded using a program modified from the MAX31855 library (Adafruit; https://github.com/adafruit/Adafruit-MAX31855-library) or the Tera Term software (https://ttssh2.osdn.jp/index.html.en).

Two-photon microscopy. The retina in the chamber was perfused with oxygenated DMEM/F12 medium using the above-mentioned perfusion system. Imaging was done with an upright multiphoton microscope system (Fluoview FV1000MPE; Olympus, Tokyo) with a water immersion objective lens (XLPLN25XWMP; Olympus). A Ti:Sapphire femtosecond laser (Mai-tai DeepSee HP; Spectra-Physics, Santa Clara, CA,

USA) was tuned at 840 nm and used for excitation. Laser power at the specimen was adjusted within 5-10 mW. The specimen was XY-scanned at 256 × 256 pixels with 8 μs of pixel dwelling time. Fluorescent emission was collected by the objective lens, filtered through a dichroic mirror RDM690 (Olympus) to block the returned excitation light, split with a set of dichroic mirrors (DM505, DM450 and DM570; Olympus), and finally filtered through bandpass filters (FF01-425/30-25; Semrock, Rochester, NY, USA; BA460-500, Olympus; BA520-560, Olympus; 645/60, Chroma, Bellows Falls, VT, USA) to separate blue (not used in this study), cyan (CFP Ch), yellow (FRET Ch) and red fluorescence (Red Ch; used only for the rhodamine-labeled image in Fig. 1*I*), respectively. Fluorescent signals were detected and amplified with multi-alkaline photomultiplier tubes to reconstruct images on FV10-ASW software version 4.2 (Olympus). Images in Fig. 3*A* and Movie S5 were created by combining four 509 μm square images which were obtained sequentially within 30 s.

Light stimulation. Stimulation light was generated with a custom-made LED system (Fig. S4). Light intensity and duration were controlled by the Arduino UNO microcontroller board connected to the LED driver, using a program written with Arduino IDE. When necessary, calibrated neutral density filters (ND filters, Fig. S4; Edmund Optics, Barrington, NJ, USA) were additionally used to attenuate the light intensity. Light wavelength was controlled by a bandpass filter (Fig. S4; Edmund Optics). Light was delivered to the retina through the objective lens. To avoid light attenuation, the dichroic mirror RDM690 before the objective lens was manually changed to a normal mirror during the stimulation. Light intensity was calibrated based on power measurements with an optical power meter (TQ8210; Advantest, Tokyo). The power in Watts was divided by the energy of a photon and illuminated area (0.68 mm^2 circle) to obtain photon density. The energy of a photon was derived from

$$E = \frac{h\nu}{\lambda}$$

where E is photon energy, h is the Planck constant ($6.62606957 \times 10^{-34}$ m^2 kg s^{-1}), c is the speed of light in a vacuum (2.99792458×10^8 m/s) and λ is wavelength (m). For short stimulations, light was delivered in 6 s just before an image acquisition, except for 6×10^{10} and 1.9×10^{11} (photons μm^{-2} s^{-1}) stimulation at both 575 and 600 nm, in which the maximal light intensity was used for 6-30 s to deliver the indicated numbers of photons. For long stimulations of 10 min (Figs. 2*E* and 6*F*), light was delivered only during the intervals of time-lapse imaging, and thus the light was temporarily turned off every 2 min during the image acquisition (< 10 s). View fields for the light response measurements were always selected from areas where the stimulation light spot had not been projected yet.

Image analyses. Images were analyzed on Fiji (https://fiji.sc). Positional drift in the time-lapse imaging was corrected with the Correct 3D drift plug-in (12). The minimum pixel intensity obtained from a blank image was used as the background signal and subtracted from every pixel. Pseudocolor PKA activity images were generated by multiplying an 8-color FRET/CFP ratio image and the corresponding intensity-normalized grayscale image (Fig. S1*B*). Longitudinal images of the retina were created by reconstruction from z-stack images. Sixteen y-slice images were averaged for noise reduction and better visualization of cellular morphology. When comparing rods and cones (Fig. 3 *F* and *G*), intensity-based segmentation was performed using a mask image that covered the cone or rod region. The mask image was created by superimposing two binary images. The first image was created using the Auto threshold function with the MaxEntropy method (13). To create the second image, a local background image was created by applying a median filter of 10 pixels diameter, and this background image was subtracted from the original image. The subtracted image was then binarized into the top 1% highest intensity pixels

and others, to obtain the second binary image. Two mask images were overlaid using the Image calculator function with the OR method. The thus-obtained mask image or its inverted image was applied to the original image to extract cone or rod signals, respectively.

Photopigment analyses. The absorbance spectrum of photopigments in the retina was obtained as described previously (4). A dark-adapted control retina was transferred into 500 µL collection buffer (140 mM NaCl, 50 mM HEPES, pH 6.5 NaOH) immediately after its collection and frozen with liquid nitrogen. A light-adapted retina was flat-mounted as described above, transferred into 500 µL collection buffer, and frozen. A frozen retina was thawed and homogenized using a 1 mL syringe (SS-01T; Terumo, Tokyo) by passing through a 23-gauge needle (NN-2325R; Terumo) and centrifuged (17,400 ×g, 15 min, 4°C). After removing the supernatant, the membrane precipitate was solubilized in 300 µL solubilization buffer (collection buffer supplemented with 1% (w/v) DDM), mixed on a rotator at 4°C for 30 min, and centrifuged (17,400 ×g, 15 min, 4°C). The supernatant was collected, supplemented with 16 µL of 5 M NH_2OH (pH 6.8, NaOH; final concentration of 100 mM), and analyzed with a spectrophotometer (UV-2400PC; Shimadzu, Kyoto) at 4°C. The difference spectrum of photopigment was obtained from absorbance data before and after an irradiation with intense yellow light passed through a Y52 filter. Molar extinction coefficients of rhodopsin (40,200 M^{-1} cm^{-1}) (14) and isorhodopsin (43,000 M^{-1} cm^{-1}) (15) were used to estimate the molar amount of each pigment after the fitting analysis in Fig. 5*D*.

Equivalent DDM-solubilized samples were also used for the HPLC analysis. Retinoid extraction and HPLC were performed as described previously (16) using an HPLC system (LC-10AT VP; Shimadzu) with a silica column (150 × 6.0 mm, A-012–3; YMC, Kyoto, Japan) and a solvent composed of 98.8% (v/v) benzene, 1.0% (v/v) diethylether, and 0.2% (v/v) 2-propanol. Each retinoid in eluate was detected by its absorbance at 360

nm. Molar ratios of retinoids were estimated by dividing the peak area with the corresponding molar extinction coefficient at 360 nm (M^{-1} cm^{-1}): 35,000 for *syn*-11-*cis* retinal oxime; 29,600 for *anti*-11-*cis* retinal oxime; 54,900 for *syn*-all-*trans* retinal oxime; 51,600 for *anti*-all-*trans* retinal oxime; 39,300 for *syn*-9-*cis* retinal oxime; 30,600 for *anti*-9-*cis* retinal oxime; 49,000 for *syn*-13-*cis* retinal oxime; 52,100 for *anti*-13-*cis* retinal oxime; and 10,900 for all-*trans* retinol.

Data fittings. Rhodopsin absorption (Fig. 5*D*) was fitted with rhodopsin and isorhodopsin templates from 450 to 600 nm by the least squares method. The rhodopsin template was experimentally obtained from the dark-adapted control retina, and the isorhodopsin template was obtained from the literature (17).

Intensity-response relationships (Fig. S3*B*) were fitted using Origin 9 (OriginLab, Northampton, MA, USA) with the Naka-Rushton equation:

$$R = R_{max}\frac{I^n}{(I^n + {I_{1/2}}^n)}$$

where R is the peak amplitude, R_{max} is the amplitude of the saturated response, I is light intensity, n is the Hill coefficient, and $I_{1/2}$ is the light intensity to generate a half-maximal response.

A spectral sensitivity plot (Fig. 4*A*) was fitted with the spectral template for the α-band of A1 pigments:

$$\mathrm{S(x)} = \frac{1}{\exp[A(a-x)] + \exp[B(b-x)] + \exp[C(c-x)] + D'}$$

where $x = \lambda_{max}/\lambda$, A = 69.7, a = 0.88, B = 28, b = 0.922, C = -14.9, c = 1.104, and D = 0.674 (3).

Supplementary Figures

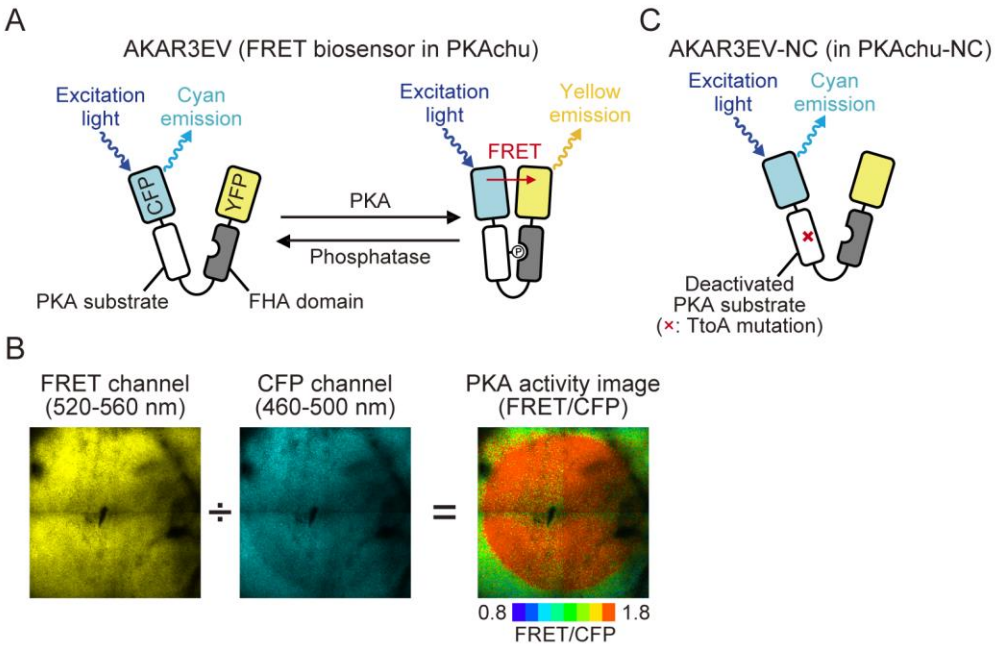

Fig. S1. Visualization of PKA activity using AKAR3EV FRET-biosensor.

(*A*) Predicted protein structure and mode of action of AKAR3EV. Activated PKA phosphorylates the threonine residue in the PKA substrate motif. Phospho-threonine is then recognized by the forkhead-associated (FHA) domain to promote FRET from cyan fluorescent protein (CFP) to yellow fluorescent protein (YFP), which increases yellow fluorescence. (*B*) Generation of a FRET/CFP ratio image to visualize PKA activity. The fluorescent emission from the PKAchu retina is separated into yellow and cyan light and received by two detectors, the FRET and CFP channels, respectively. The intensity of each pixel in the FRET channel image is divided by that of the CFP channel image to generate an 8-color FRET/CFP ratio image (see the *Supplementary Methods* for detail). Sample images are obtained from light-stimulated photoreceptor cells (Fig. 3A). (*C*) AKAR3EV-NC for the negative control. The PKA phosphorylation site, threonine, is substituted to alanine so that FRET efficiency is not affected by PKA.

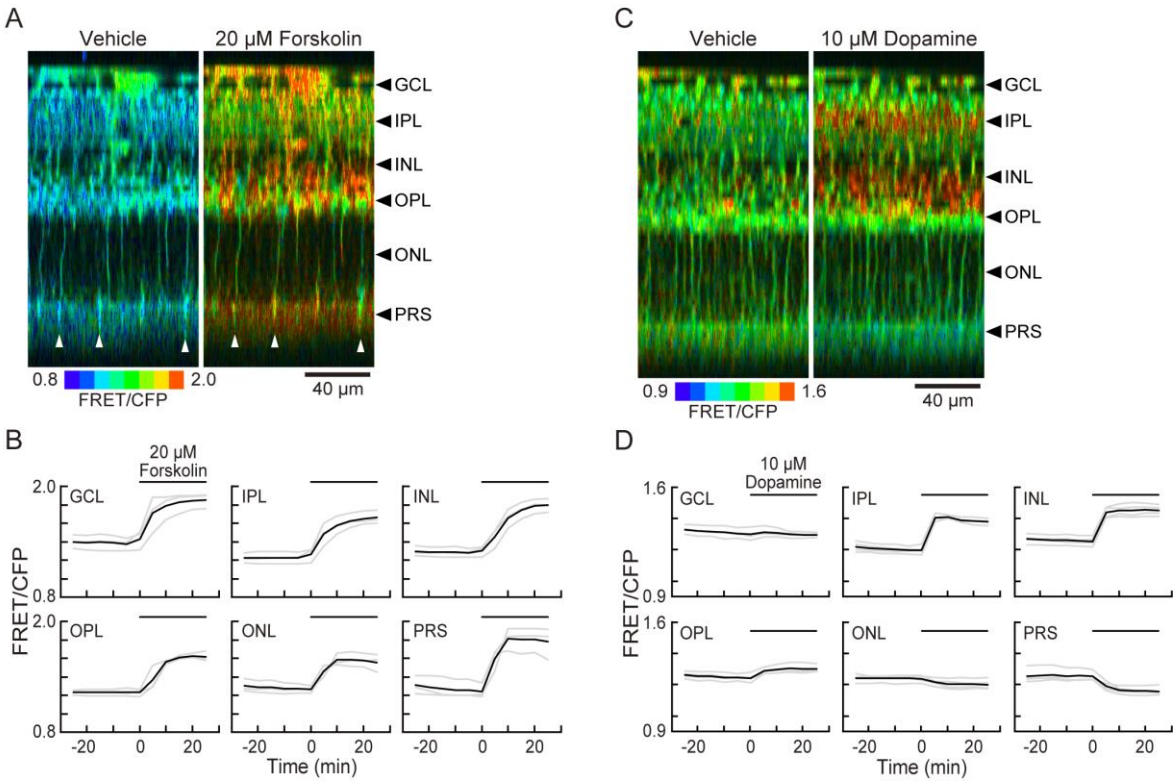

Fig. S2. Forskolin and dopamine responses in the PKAchu retina.

(*A*) Longitudinal images of the PKA activity before and after the perfusion of 20 μM forskolin. Images were reconstructed from a z-stack of 43 images with 4.5 μm z-intervals. White arrowheads indicate cones. Black arrowheads indicate the positions of the layers analyzed in *B*. (*B*) Time courses of forskolin-induced PKA activations at each layer. (*C*) Longitudinal images of the PKA activity before and after the perfusion of 10 μM dopamine. Images were reconstructed from a z-stack of 40 images with 5 μm z-intervals. (*D*) Time courses of dopamine-induced PKA activity changes at each layer. For both *B* and *D*, data points were obtained every 5 min and horizontal bars show the timing of drug perfusion. Light-colored and dark-colored curves are individual and averaged data, respectively. n = 3 and 4 for forskolin and dopamine, respectively.

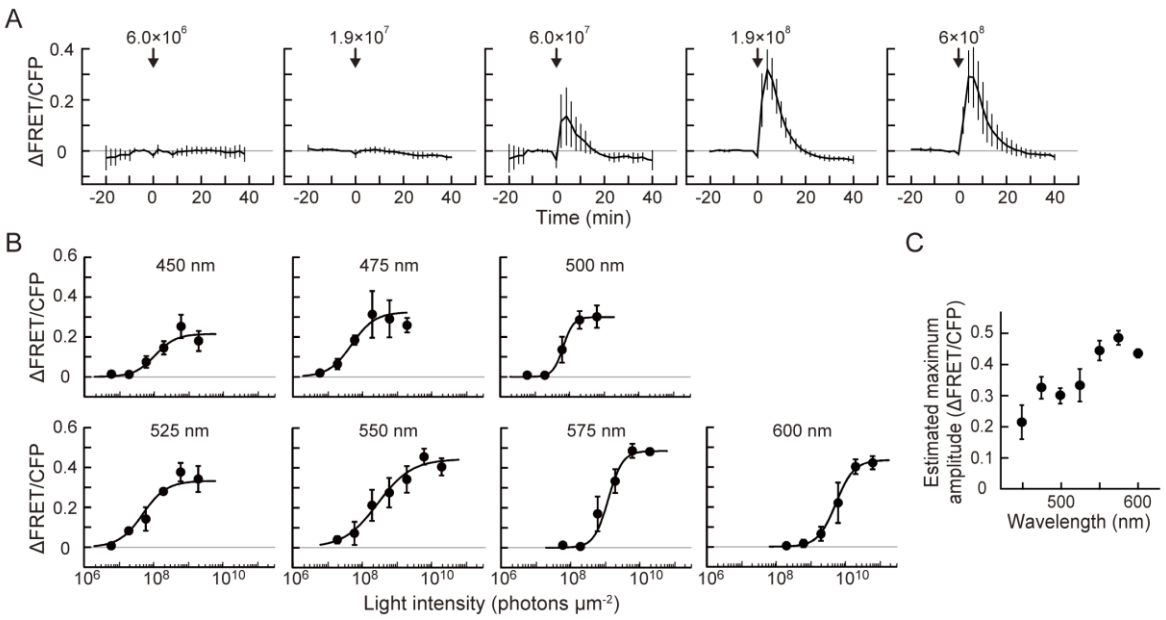

Fig. S3. Intensity-response relationships of the light-off-induced PKA activation.

(*A*) Rod responses toward a 6 s stimulation of various intensities of light at 500 nm. Numbers indicate the light intensity (photons μm^{-2}) and arrows indicate the timing of the stimulation. Data were obtained every 2 min. Values are the mean ± SD (n = 3). (*B*) Intensity-response relationships of the light-off-induced PKA activation at each indicated wavelength. Values are the mean ± SEM (n = 3 to 7). (*C*) Relationship between the estimated maximum response amplitude and wavelength of the stimulation light. Values are the mean ± SEM (n = 3 to 7).

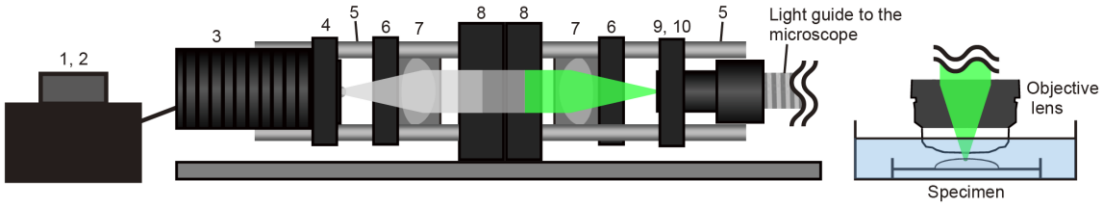

Components

Number	Component	Catalog number*	Quantity
1	Power supply	TPS001	1
2	LED driver	LEDD1B	1
3	White LED	MNWHL4	1
4	Cage plate	CP12	1
5	Cage assembly rods	ER3-P4	2
6	Cage plate	CP02/M	2
7	Lens	AC254-030-A-ML	2
8	Sliding filter mount	CFS1/M	2
9	Optic mount	CXY1	1
10	Adaptor	AD15F	1

*Thorlabs

Filters used in the component #8

Product name	Catalog number*
400, 450, 500, 550, 600, 650 and 700 nm bandpass filter kit	#88-300
425 nm bandpass filter	#87-787
475 nm bandpass filter	#87-788
525 nm bandpass filter	#87-789
575 nm bandpass filter	#87-790
625 nm bandpass filter	#87-791
675 nm bandpass filter	#87-792
ND1 filter	#48-090
ND2 filter	#48-092
ND3 filter	#48-093
ND4 filter	#36-273

*Edmund optics

Fig. S4. Custom-made LED light stimulation system.

Layout of the system. Numbers indicate the components listed below. Filters used in component #8 are also listed.

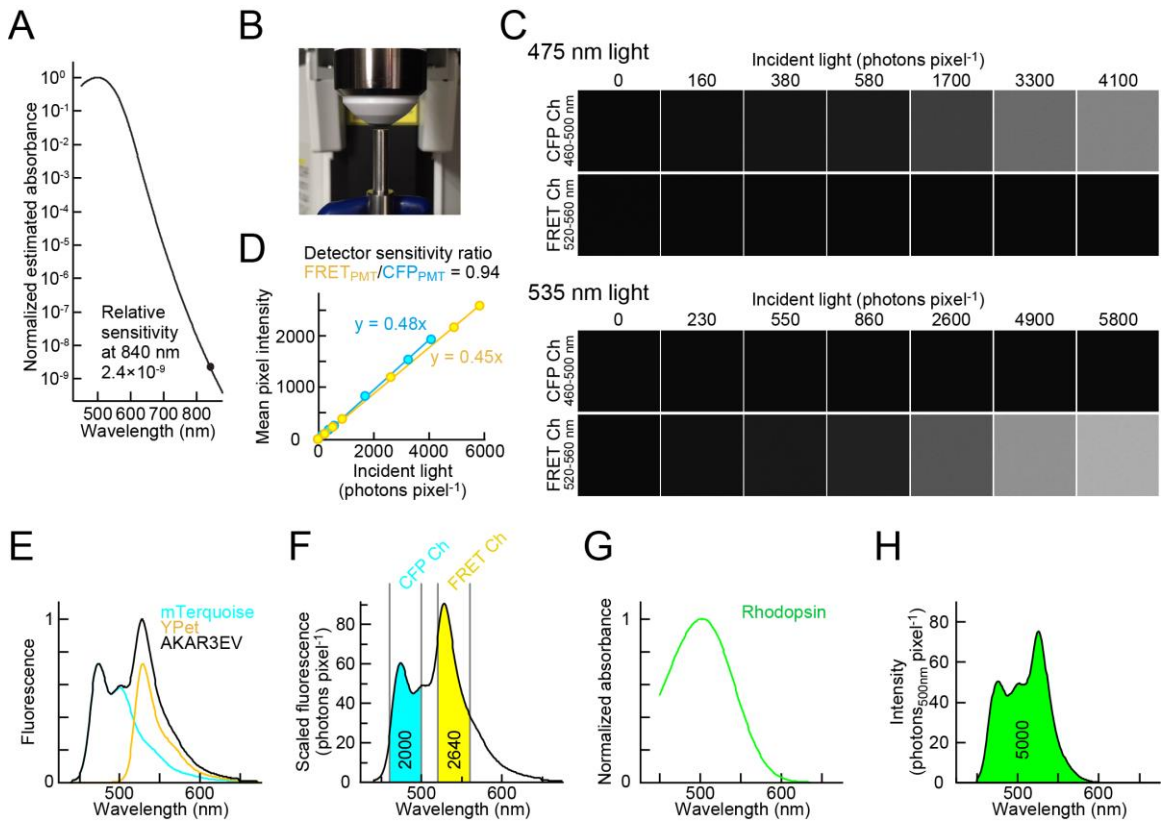

Fig. S5. Estimation of the amount of photopigment activation during two-photon imaging.

(*A*) The rhodopsin absorbance template extended to the infrared wavelength. (*B*) A picture of the photon injection setup. (*C*) Images obtained with CFP Ch and FRET Ch detectors when injecting indicated number of photons at 475 nm (upper panels) or 535 nm (lower panels). (*D*) Relationships of incident light intensity and mean pixel intensity of images. (*E*) A predicted emission spectrum of AKAR3EV. (*F*) A scaled spectrum. Numbers show areas of colored regions. (*G*) The normalized absorbance spectrum of rhodopsin. (*H*) A spectrum obtained by multiplying *F* by *G*. The number is the area of green region.

Legends for Supplementary Movies

Movie S1 (separate file) Z-stack images of the PKAchu retina. Two hundred cross-sectional images were obtained in a 105 μm square area with 1 μm z-intervals.

Movie S2 (separate file) Three-dimensional reconstruction of PNA-labeled photoreceptors. PNA-labeled cone sheaths (magenta) and AKAR3EV^{high} cells (green) were imaged.

Movie S3 (separate file) Forskolin response of the PKAchu retina. Longitudinal images were reconstructed from 43 cross-sectional images with 4.5 μm z-intervals. The time-lapse interval was 5 min. Forskolin was continuously delivered from time 0.

Movie S4 (separate file) Dopamine response of the PKAchu retina. Longitudinal images were reconstructed from 40 cross-sectional images with 5 μm z-intervals. Dopamine was continuously delivered from time 0.

Movie S5 (separate file) The light-off-induced PKA activation after a 10 min-stimulation. Data were obtained from a retinal explant prepared from the light-adapted PKAchu. Images are cross-sectional views from the PRS layer. Light stimulation (500 nm, 3.2×10^7 photons μm^{-2} s^{-1}) was given from -10 to 0 min. The time-lapse interval was 2 min.

Movie S6 (separate file) Responses in PKAchu and PKAchu-NC retinal explants toward a 6 s-light stimulation. Images are cross-sectional views from the PRS layer. Stimulation light (500 nm, 1.0×10^8 photons μm^{-2} s^{-1}) was projected just before time 0 at the center of the view field indicated as dashed circles. The time-lapse interval was 2 min.

Movie S7 (separate file) Cell-type specificity of the light-off-induced PKA activation. Longitudinal images were reconstructed from 35 cross-sectional images with 5 μm z-intervals. A 6 s light stimulation (500 nm, 1.0×10^8 photons μm^{-2} s^{-1}) was given just before time 0.

Movie S8 (separate file) High-magnification cross-sectional images of the light-off-induced PKA activation at the PRS layer. A 6 s light stimulation (500 nm, 1.0×10^8 photons μm^{-2} s^{-1}) was given just before time 0. Note that bright spots are cones.

Movie S9 (separate file) Comparison of the light-induced PKA activity changes between wild-type and albino PKAchu photoreceptor cells. Images are cross-sectional views from the PRS layer. Wild-type data are those used in Movie S5. Light stimulation (500 nm, 3.2×10^7 photons μm^{-2} s^{-1}) was given from -10 to 0 min.

SI References

1. T. Euler, K. Franke, T. Baden, "Studying a light sensor with light: multiphoton imaging in the retina" in Multiphoton Microscopy, E. Hartveit, Ed. (Humana Press, 2019), vol. 148, chap. 10, pp. 225-250.
2. G. Palczewska *et al.*, Human infrared vision is triggered by two-photon chromophore isomerization. *Proc Natl Acad Sci U S A* **111**, E5445-5454 (2014).
3. V. I. Govardovskii, N. Fyhrquist, T. Reuter, D. G. Kuzmin, K. Donner, In search of the visual pigment template. *Vis Neurosci* **17**, 509-528 (2000).
4. K. Sakurai *et al.*, Physiological properties of rod photoreceptor cells in green-sensitive cone pigment knock-in mice. *J Gen Physiol* **130**, 21-40 (2007).
5. P. H. M. Bovee-Geurts, J. Lugtenburg, W. J. DeGrip, Coupled HOOP signature correlates with quantum yield of isorhodopsin and analog pigments. *Biochim Biophys Acta Bioenerg* **1858**, 118-125 (2017).
6. M. J. Mattapallil *et al.*, The Rd8 mutation of the Crb1 gene is present in vendor lines of C57BL/6N mice and embryonic stem cells, and confounds ocular induced mutant

phenotypes. *Invest Ophthalmol Vis Sci* **53**, 2921-2927 (2012).
7. N. Le Fur, S. R. Kelsall, B. Mintz, Base substitution at different alternative splice donor sites of the tyrosinase gene in murine albinism. *Genomics* **37**, 245-248 (1996).
8. P. D. Calvert *et al.*, Phototransduction in transgenic mice after targeted deletion of the rod transducin alpha -subunit. *Proc Natl Acad Sci U S A* **97**, 13913-13918 (2000).
9. E. Ivanova, A. H. Toychiev, C. W. Yee, B. T. Sagdullaev, Optimized protocol for retinal wholemount preparation for imaging and immunohistochemistry. *J Vis Exp* 10.3791/51018, e51018 (2013).
10. L. Bhatt, G. Groeger, K. McDermott, T. G. Cotter, Rod and cone photoreceptor cells produce ROS in response to stress in a live retinal explant system. *Mol Vis* **16**, 283-293 (2010).
11. P. R. Williams, J. L. Morgan, D. Kerschensteiner, R. O. Wong, In vitro imaging of retinal whole mounts. *Cold Spring Harb Protoc* **2013** (2013).
12. A. Parslow, A. Cardona, R. J. Bryson-Richardson, Sample drift correction following 4D confocal time-lapse imaging. *J Vis Exp* 10.3791/51086 (2014).
13. J. N. Kapur, P. K. Sahoo, A. K. C. Wong, A new method for gray-level picture thresholding using the entropy of the histogram. *Comput Vision Graph* **29**, 273-285 (1985).
14. H. Imai *et al.*, Molecular properties of rhodopsin and rod function. *J Biol Chem* **282**, 6677-6684 (2007).
15. T. Yoshizawa, G. Wald, Pre-lumirhodopsin and the bleaching of visual pigments. *Nature* **197**, 1279-1286 (1963).
16. K. Sato *et al.*, Opn5L1 is a retinal receptor that behaves as a reverse and self-regenerating photoreceptor. *Nat Commun* **9**, 1255 (2018).
17. J. Fan, B. Rohrer, G. Moiseyev, J. X. Ma, R. K. Crouch, Isorhodopsin rather than rhodopsin mediates rod function in RPE65 knock-out mice. *Proc Natl Acad Sci U S A* **100**, 13662-13667 (2003).